

# Long Term Motion Prediction Using Keyposes

Sena Kiciroglu<sup>1</sup> Wei Wang<sup>1,2</sup> Mathieu Salzmann<sup>1,3</sup> Pascal Fua<sup>1</sup>

<sup>1</sup> CVLab, EPFL, Switzerland    <sup>2</sup> University of Trento, Italy    <sup>3</sup> ClearSpace, Switzerland

## Abstract

*Long term human motion prediction is essential in safety-critical applications such as human-robot interaction and autonomous driving. In this paper, we show that, to achieve long term forecasting, predicting human pose at every time instant is unnecessary. Instead, it is more effective to predict a few keyposes and approximate intermediate ones by linearly interpolating the keyposes.*

*We will demonstrate that our approach enables us to predict realistic motions for up to 5 seconds in the future, which is far larger than the typical 1 second encountered in the literature. Over this extended time period, our predictions are more realistic and better preserve the motion dynamics than those state-of-the-art methods yield.*

*Furthermore, because we model future keyposes probabilistically, we can generate multiple plausible future motions by sampling at inference time. This is useful to model because people usually can do one of several things given what they have already done.*

## 1. Introduction

Human motion prediction is a key component of many vision-based applications, such as automated driving [14, 10], surveillance [25, 17], accident prevention [29], and human-robot interaction [13, 6]. Its goal is to forecast the future 3D articulated motion of a person given their previous 3D poses. Most current approaches formulate this task as one of regressing a person’s pose in every future frame of a sequence given the current ones. Recurrent neural networks (RNNs) [12, 23] and graph convolutional networks (GCNs) [22, 18, 21] have proven effective for this, at least for short-term predictions, typically up to one second in the future. However, beyond one second, the predictions degrade quickly, and very little work has aimed to address this shortcoming.

This paper focuses on longer-term predictions. Our key insight is that predicting the pose in *every* future frame is unnecessary because, given two poses separated by a short time interval, one can easily guess the intermediate ones

using simple linear interpolation. It is therefore enough to predict a set of *keyposes* from which all others can be recovered by interpolation. Such keyposes are by definition sparser than the full set of future poses and therefore easier to forecast.

In practice, we learn keyposes from training data. We take them to be a subset of poses within a set of motions from which all other poses can be linearly interpolated up to a fixed precision. While all keyposes are unique, some of them tend to be similar to each other, which allows us to cluster them. Predicting future motions can then be reformulated as jointly classifying to which cluster the future keyposes belong and regressing the time interval between successive ones. To this end, we design an RNN-based motion prediction network that takes earlier keyposes as input and yields a probability distribution over the clusters for each future keypose along with transition times. As a result, we can not only predict the most likely future motion by maximizing cluster probabilities but also generate multiple potential futures by sampling these probability distributions. This is useful because people are not entirely predictable, even when one knows what they have already done, as in the case of a pedestrian standing on the curb who may, or may not, cross the street.

We will demonstrate that our approach enables us to predict multiple realistic motions for up to 5 seconds in the future, which is far larger than the typical 1 second encountered in the literature. Unlike state-of-the-art methods that were designed for this shorter timespan, the motions we generate preserve the dynamic nature of the observations, whereas the SOTA ones tend to degenerate towards static poses.

## 2. Related Work

The complexity of human motion makes deep learning an ideal framework for tackling the task of motion prediction. In this section, we first review the two main classes of deep models that have been used in the field and then discuss approaches that depart from these main trends.

## 2.1. Human Motion Prediction using RNNs

Recurrent neural networks (RNN) are widely used architectures for modeling time-series data, for instance for natural-language processing [32] and music generation [28, 27]. Since the work of Fragkiadaki *et al.* [11], these architectures have become highly popular for human motion forecasting. In this context, the S-RNN of Jain *et al.* [16] transforms spatio-temporal graphs to a feedforward mixture of RNNs; the Dropout Autoencoder LSTM (DAE-LSTM) of Ghosh *et al.* [12] synthesizes long-term realistic looking motion sequences; the recent Generative Adversarial Imitation Learning (GAIL) of Wang *et al.* [31] was employed to train an RNN-based policy generator and critic networks. HP-GAN [3] uses an RNN-based GAN architecture to generate diverse future motions of 30 frames.

Despite their success, using RNNs for long-term motion prediction suffers from drawbacks. As pointed out by Martinez *et al.* [23] they tend to produce discontinuities at the transition between observed poses and predicted ones and often yield predictions that converge to the mean pose of the ground-truth data in the long term. In [23], this was circumvented by adding a residual connection so that the network only needs to predict the residual motion of the subject. Here, we also develop an RNN-based architecture. However, because we treat keypose prediction as a classification task, our approach will not suffer from the accumulated error that such models tend to generate when employed for regression.

## 2.2. Human Motion Prediction using GCNs

Mao *et al.* [22] proposed to overcome the weaknesses of RNNs by encoding motion in discrete cosine transform (DCT) space, to model temporal dependencies, and learning the relationships between the different joints via a GCN. Lebailly *et al.* [18] build on top of this work by combining a GCN architecture with a temporal inception layer. The temporal inception layer serves to process the input at different subsequence lengths, so as to exploit both short-term and long-term information. Alternatively, “History Repeats Itself” [21] combines the GCN architecture with an attention module aiming to learn the repetitive motion patterns. These methods constitute the state of the art for long-term prediction. Nevertheless, they were only showcased for forecasting up to 1 second in the future. As will be shown by our experiments, for longer timespans, they tend to degenerate to static predictions.

## 2.3. Other Human Motion Prediction Approaches

Several other architectures have been proposed for human motion prediction. For example, Bütepage *et al.* [5] employ several fully-connected encoder-decoder models to encode different properties of the data. One of the models is a time-scale convolutional encoder, with different filter

sizes. In [6], a conditional variational autoencoder (CVAE) is used to probabilistically model, predict and generate future motions. This probabilistic approach is extended in [7] to incorporate hierarchical action labels. Aliakbarian *et al.* [1] also perform motion generation and prediction by encoding their inputs using a CVAE. They are able to generate diverse motions by randomly sampling and perturbing the conditioning variables. Li *et al.* [19] use a convolutional neural network for motion prediction, producing separate short-term and long-term embeddings. In [9], interactions between humans and objects in the scene are learned for context-aware motion prediction, which enables predictions for up to 2 seconds but depends on interactions with objects, which is beyond our scope. In any event, all the above-mentioned methods aim to regress the future poses at every time instant. Here, we will show that this is unnecessary, and that truly long-term prediction can be achieved more accurately by focusing the prediction on the essential poses, or keyposes, in a sequence.

## 3. Methodology

Classically, the task of motion prediction is defined as producing the sequence of 3D poses from  $t = 1$  to  $t = N$ , denoted as  $\mathbf{P}_{1:N}$ , given the sequence of poses from  $t = -M$  to  $t = 0$ , denoted as  $\mathbf{P}_{-M:0}$ . Each pose value  $\mathbf{P}_t$  is of dimension  $3 \times J$ , where  $J$  is the total number of joints. Therefore, pose-to-pose prediction can be written as

$$\mathbf{P}_{1:N} = F(\mathbf{P}_{-M:0}),$$

where  $F$  is the prediction function.

Our approach departs from this classical formalism by predicting keyposes from keyposes. A keypose  $\mathbf{K}_i$  is defined as a triplet containing a keypose value, label and duration, denoted as  $(\mathbf{V}_i, l_i, d_i)$ , where  $i \in [1, I]$ , and  $I$  is the total number of keyposes in a sequence. Each keypose value  $\mathbf{V}_i$  is of dimension  $3 \times J$ . Let us assume for now that we have extracted keypose values for the training data, and that we have clustered these keypose values into  $C$  clusters. We will discuss in Section 3.1 our approach to doing so. Then, the keypose label  $l_i \in [1, C]$  indicates which cluster the keypose falls into. Finally, the duration  $d_i$  is the number of transition frames from  $\mathbf{K}_{i-1}$  to  $\mathbf{K}_i$ .

Therefore, our keypose-to-keypose framework takes as input a motion  $\mathbf{P}_{-M:0}$  defined by its keyposes  $\mathbf{K}_{-I_1:0}$ , where  $I_1$  is the number of keyposes in the past sequence. We then aim to predict  $\mathbf{K}_{1:I_2}$ , where  $I_2$  is the number of keyposes in the future sequence. We write this as

$$\mathbf{K}_{1:I_2} = G(\mathbf{K}_{-I_1:0}),$$

where  $G$  is the keypose-to-keypose prediction function.

In practice, we do not predict the keypose values  $\mathbf{V}_{1:I_2}$ , but only the labels  $l_{1:I_2}$ . To then obtain the  $d_{i+1}$  poses between keyposes  $\mathbf{K}_i$  and  $\mathbf{K}_{i+1}$ , we perform linear interpolation between the keypose cluster centers  $\mathbf{C}_{l_i}$  and  $\mathbf{C}_{l_{i+1}}$ . This yields

$$\mathbf{P}_{\Delta t+t} = \mathbf{C}_{l_i} + \Delta t \frac{\mathbf{C}_{l_{i+1}} - \mathbf{C}_{l_i}}{d_{i+1}},$$

where  $t$  is the time index of keypose  $\mathbf{K}_i$  in the sequence.

Note that we use a 3D joint position representation of human motion. This representation has been gaining popularity over Euler angles, due to the latter suffering from ambiguities. Specifically, two different sets of angles can represent the same pose. Consequently, the interpolation between poses represented by angles becomes ambiguous as well. Recent approaches have tried to solve this by changing the encoding to quaternions [26], but many works nonetheless report results using the 3D joint position representation [22, 18, 21].

### 3.1. Keyposes

Given a sequence of poses  $\mathbf{P}_t, t \in [1, T]$  where  $T$  is the length of the sequence, we seek to retrieve the keyposes  $\mathbf{K}_i, i \in [1, I]$ . We employ an optimization based strategy to determine the poses which minimizes the L2 error between the original sequence  $\mathbf{P}$  and the sequence reconstructed by linear interpolation.

Our method is as follows:

- We set  $\mathbf{P}_1$  and  $\mathbf{P}_T$  to be keyposes.
- We recursively subdivide the time window spanned by  $\mathbf{P}$ , where each split selects the pose  $\mathbf{P}_t$  at position  $t$  which has the highest L2 error with respect to the pose reconstructed by linear interpolation at the same time index. The recursion ends once the error is below a threshold, yielding an initial set of keyposes.
- The set of keyposes is further refined by optimizing for the time indices of the keyposes and the keypose values themselves. The optimization aims to minimize the L2 error between the original sequence and the sequence reconstructed by interpolating the keyposes.

The keyposes are extracted for every training motion individually and collected in one set which is then clustered into  $K$  clusters via k-means. Each keypose is given a label determined by the cluster it is assigned to. Finally, we prune the keyposes by removing the unnecessary intermediate ones that have the same label as their preceding and succeeding keypose. Pruning is illustrated in Figure 1. An example distribution of keyposes in a sequence is shown in Figure 2.

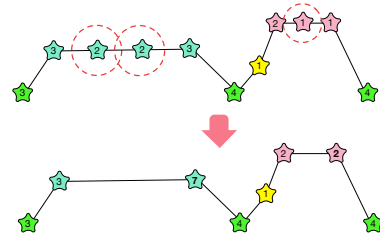


Figure 1. **Illustration of keypose pruning.** The top figure depicts the sequence before pruning. The keyposes are shown as stars, with their color indicating their label and the number inside indicating their duration. The keyposes to be pruned are circled. The bottom figure shows the sequence after pruning. The keyposes following the pruned ones have increased duration. Note that the same sequence can be reconstructed from both the pruned and unpruned keyposes, as there is no loss of information.

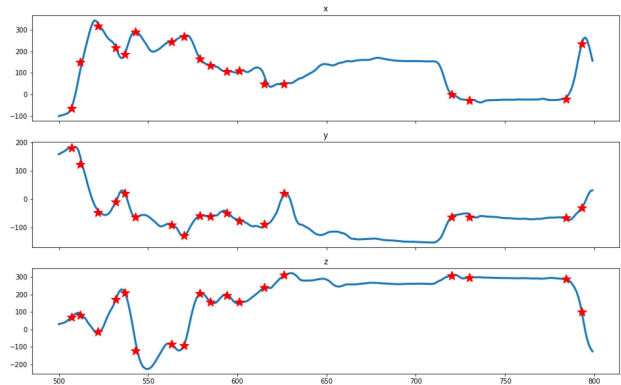


Figure 2. **Distribution of keyposes** in a short sequence. The plots depict the x, y, and z coordinates of the right wrist of subject 1 during the smoking action. We depict the locations of the keyposes as red stars. The keyposes are distributed more where the motion is the most varied and these keyposes have shorter duration.

### 3.2. Motion Prediction Framework

We have designed an RNN based neural network as our keypose-to-keypose prediction framework, as shown in Figure 3. The inputs to the network for step  $i$  are the tokenized keypose label  $L_i$  and the keypose duration distribution  $D_i$  discussed below. We tokenize the labels in the following steps.

1. If we know the keypose value: We compute the negative distances between the keypose value  $\mathbf{V}_i$  and all cluster centers  $\mathbf{C}_j, j \in [1, C]$ .
2. If we do not know the keypose value (i.e., during inference): We compute the negative distances between the keypose cluster center of label  $i, \mathbf{C}_{l_i}$ , and all cluster centers  $\mathbf{C}_j, j \in [1, C]$ .

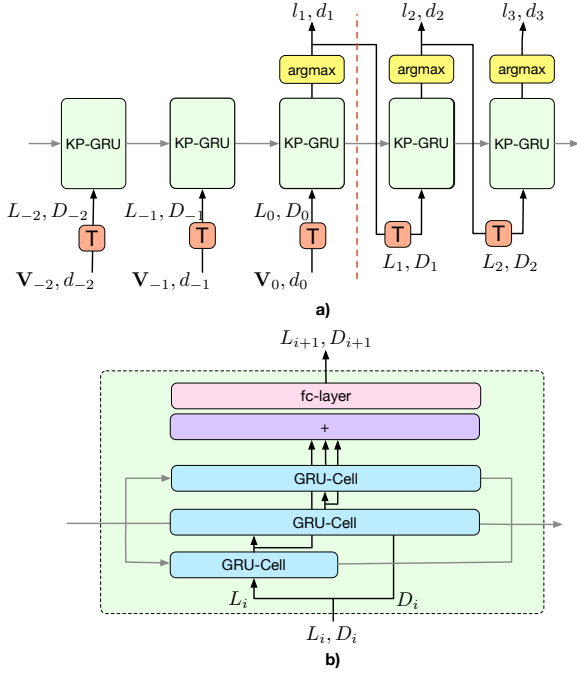


Figure 3. **Keypose-to-keypose network structure.** Figure a) depicts our overall architecture. At step  $i$ , pairs of tokenized keypose labels and durations,  $L_i, D_i$  are fed to the keypose GRU (KP-GRU) unit and the labels and durations of step  $i + 1$  are predicted. The present is depicted at  $i = 0$ . Before this time-step, the network is given ground truth keyposes as conditioning. The tokenized label  $L_i$  is found using the keypose value  $V_i$ . After time-step  $i = 0$ , the network is given its own predictions as input rather than the ground truth. The tokenized label  $L_i$  is found using the predicted label  $l_i$ . The orange T blocks represent the tokenization operation. Figure b) depicts the inner structure of the KP-GRU unit, which consists of a three layer GRU network followed by a fully connected layer.

3. We pass the resulting negative distances through a softmax operation with a temperature of 0.03.

Note that tokens sum up to 1 and can be thought of as a probability distribution over labels.

To obtain a duration distribution  $D_i$ , we also categorize the durations into very short (less than 4 frames), short (between 5 and 10 frames), medium (between 10 and 14 frames), long (between 14 and 25 frames), and very long (more than 25 frames).

The network predicts a pair of distributions: over the labels and over the duration categories. We train the network using three different loss functions:

- $E_{\text{ce-soft}}$ : The cross-entropy loss between the ground-truth tokenized label and the predicted distribution over the labels to be used as a soft loss,

- $E_{\text{ce-hard}}$ : The cross-entropy loss between the ground-truth label and the predicted label distribution to be used as a hard loss,
- $E_{\text{duration}}$ : The cross-entropy loss between the predicted duration distribution and the ground-truth duration category.

The overall loss is

$$E = w_{\text{ce-soft}} E_{\text{ce-soft}} + w_{\text{ce-hard}} E_{\text{ce-hard}} + w_{\text{dur}} E_{\text{duration}}, \quad (1)$$

where  $w_{\text{ce-soft}}$ ,  $w_{\text{ce-hard}}$ ,  $w_{\text{dur}}$  are the weights corresponding to the different loss terms.

The loss is not only enforced on the future predictions, but also on the outputs of the network as it processes the conditioning ground truth. For these past time steps, the loss is multiplied by a factor of  $i/I_1$ , where  $i$  is the prediction step and  $I_1$  is the number of past keyposes in the sequence. This factor is small in the beginning of the sequence, where we do not have enough past frames to base the future prediction on. As the amount of past frames increase, the loss factor gets larger, until it reaches 1.

During training, the label of the next keypose  $l_{i+1}$  is determined as the one with the highest predicted probability. This label is tokenized before being fed back to the network. This procedure prevents error accumulation as the prediction progresses and guarantees that the network will never see anything very different from what it was trained on. The duration of the next keypose  $d_{i+1}$  is determined similarly: According to the category with the highest probability, the following value is set to 3 for very-short, 6 for short, 12 for medium, 16 for long, and 25 for very long.

Our network yields tokens for the keypose labels, which can be treated as probability distributions. Hence, at inference time, for each iteration of the recurrent network, we can sample the future label and duration from the predicted distributions. In practice, before sampling, we smooth the predicted distributions via a softmax with a temperature of 0.3. This sampling scheme allows us to produce multiple future sequences given a single observation.

### 3.3. Implementation and Training Details

We use a 3 layer GRU, depicted in Figure 3. The GRU cells all have hidden states of size 512. A Gaussian noise of magnitude 0.1 is added to the negative distances during training, to increase robustness and prevent overfitting. Furthermore, to gradually teach the network to process its own samples, we use scheduled sampling for teacher forcing, as proposed in [4]. During training, we observe 7 past keyposes and predict 12 future keyposes. At test time, we predict until we reach 5 seconds. The weights of the loss terms are set to  $w_{\text{ce-hard}} = 1.0$ ,  $w_{\text{ce-soft}} = 1.0$ ,  $w_{\text{dur}} = 0.1$ . Our network is trained for 100 epochs using a batch size of 64.

We use an Adam optimizer with a learning rate of 0.0001 and a 0.01 weight decay. We report the results of the model with the highest validation score.

## 4. Results

### 4.1. Datasets

**Human3.6M** [15] is a standard 3D human pose dataset and has been widely used in the motion prediction literature [24, 16, 22]. It contains 15 actions performed by 7 subjects. The actions are *walking, eating, smoking, discussion, directions, greeting, phoning, posing, purchases, sitting, sitting down, taking photo, waiting, walking dog and walking together*. Human pose is represented using the 3D coordinates of 32 joints. As previous work [22, 18, 21], we load the exponential map representation of the dataset, remove global rotation and translation, and generate the Cartesian 3D coordinates of each joint mapped onto a uniform skeleton. Subject 5 is reserved for testing, subject 11 for validation and the remaining subjects are used for training. We test each method on the same 64 sequences formed using indices randomly selected from Subject 5’s sequences. Note that the observed keyposes are extracted using the sequence only up to the present time index as opposed to the entire sequence. The threshold used for keypose extraction is 500mm, and we cluster the keyposes into 1000 clusters.

**CMU Mocap** [8] is another standard benchmark dataset for motion prediction and was used in [19, 22, 18]. As explained in [19] eight action categories with enough trials are used for motion prediction. We used six out of eight actions, *basketball, basketball signal, directing traffic, jumping, soccer, and wash window*, as the sequences for *running and walking* were too short to provide enough input keyposes for our method. One sequence of each action is reserved for testing, one for validation and the rest are used in training. The dataset is loaded as an exponential map representation and processed in the same manner as Human3.6M. The threshold used for keypose extraction is 250mm, as some sequences are quite short, and we found that extracting more keyposes increases validation accuracy. We cluster the keyposes into 100 clusters, as this dataset is much smaller than Human3.6M and contains only 6 action classes as opposed to 15.

### 4.2. Baselines

We selected the following baselines for comparison purposes: HisRep [21] and TIM-GCN [18] constitute the SOTA among the methods designed for long-term prediction. For HisRep, we evaluate two versions. The first one, HisRep10, was presented as the best model in [21]. It is trained to output 10 frames and iteratively use the predicted frames as input for longer term prediction. We also evaluate HisRep125, which directly predicts 125 frames by tak-

ing 150 past frames as input. For TIM-GCN, we trained a model that observes subsequences of lengths 10, 50 and 100 and predicts 125 frames, hence tailoring the architecture to longer-term predictions of 5 seconds. Finally we compare against MixAndMatch [1], the SOTA method for multiple long-term motion prediction. We trained MixAndMatch to predict 125 future frames using 100 past frames. For all baselines we used the model that gave the best validation accuracy, to be consistent with our model selection strategy.

### 4.3. Metrics

The mean per-joint position error (MPJPE) is the most popular metric to evaluate prediction quality. Unfortunately, it is ill-suited to long-term prediction because there are many possibilities for what one might do next. As a result, a long-term prediction may be very plausible but nevertheless different from what the person actually did. The MPJPE results we report in Table 1 illustrate this. Our method does well compared to the others but none of these results is particularly good. Interestingly, simply taking the mean-pose of the sequence’s action category as the prediction gives a perfectly respectable result compared to the baselines, which indicates how little discriminative power this metric has.

	best (mm)	average (mm)
Mean-Pose	194	-
Static	208	-
TIM-GCN	196	-
HisRep10	201	-
HisRep125	<b>191</b>	-
MixAndMatch	224	237
Ours	199	<b>236</b>

Table 1. Mean per joint position error (MPJPE) on the Human3.6M dataset at 5 seconds. We present the results of single prediction methods TIM-GCN[18] and HisRep[21] as their “best”. For the diverse prediction methods of MixAndMatch[1] and Ours, we present the MPJPE of the motion predicted with the lowest error (best) and the average MPJPE of all predicted multiple motions (average). None of the methods do particularly well at 5 seconds. It is also interesting to note that predicting the mean pose of each action category (Mean-Pose) and predicting the last seen pose (static) also achieve similar results on this metric, despite not being proper prediction methods. Therefore, we conclude that MPJPE is not suitable for evaluating very long term motion sequences.

As in [12], we therefore evaluate the quality and plausibility of the generated motions by passing them through an action classifier trained to predict the action category of a given motion. In our context, if the predicted motion is plausible, such a classifier should output the correct class.

To this end, we use a classifier based on the architecture of [20]. Specifically, to focus our evaluation on the quality of the predicted *motions*, we design a Motion-Only Action

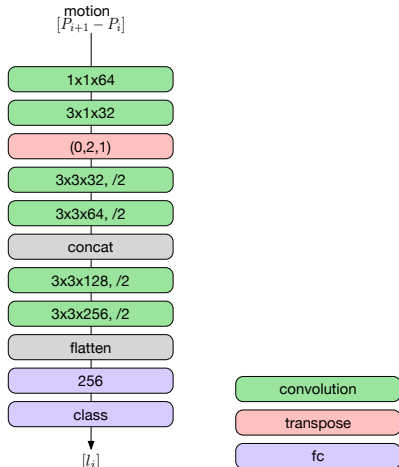


Figure 4. **MOAC architecture used for action recognition models** based on [20]. This classifier takes the motion (difference between consecutive poses) as input.

Classifier (MOAC), which takes as input motions encoded as the difference between poses in consecutive time-steps. Note that, in the supplementary material, we also report the results of a Full Action Classifier (FAC), which takes as input not only the motion as described above, but also the actual predicted 3D poses via a separate stream. However, as shown by the corresponding results, by focusing on poses, FAC can accurately predict the action category even when given a single static pose, which does not constitute a valid motion prediction.

The MOAC architecture is provided in Figure 8. We have trained it on the training sequences of Human3.6M and CMU-Mocap separately. Below, we report the top-K action recognition accuracy obtained with this classifier. For our method and for MixAndMatch, which can output multiple future predictions, we report the average accuracy over 100 predictions.

#### 4.4. Comparative Results

We compare our approach to the baselines on Human3.6M and CMU Mocap in Tables 2 and 3. In both cases, our method outperforms the others by a large margin. Fig. 5 depicts qualitative results for the greeting, purchases, waiting and walking actions of Human3.6M. Close visual inspection reveals that, while all methods work reasonably well on cyclic motions such as walking, ours does better on the acyclic ones, such as waiting. It produces wider motion ranges than the others that tend to predict less dynamic motions. Fig. 6 depicts qualitative results for multiple predictions. Our method is capable of generating diverse, yet still plausible motions.

	top-1	top-2	top-3	top-5
oracle	0.51	0.70	0.79	0.91
TIM-GCN	0.16	0.26	0.36	0.55
HisRep10	0.21	0.32	0.39	0.53
HisRep125	0.20	0.32	0.44	0.60
MixAndMatch (ave)	0.18	0.32	0.45	0.61
Ours (ave)	<b>0.33</b>	<b>0.45</b>	<b>0.55</b>	<b>0.70</b>

Table 2. **Results of the motion-only action classifier (MOAC) on the Human3.6M dataset.** We compare the classification accuracies of the motion predicted via our work compared to various versions of HisRep[21], TIM-GCN[18] and MixAndMatch[1]. We also report the accuracies of the oracle, which evaluates ground truth future motions, as an upper bound. We report the top-1, top-2, top-3 and top-5 accuracies. The results indicate that the motion predicted by our keypose network is more realistic than the motion predicted by the competing methods.

	top-1	top-2	top-3	top-5
TIM-GCN	0.44	0.69	0.85	0.95
HisRep10	0.42	0.54	0.62	0.88
HisRep125	0.34	0.48	0.57	0.82
MixAndMatch (ave)	0.30	0.39	0.58	0.85
Ours (ave)	<b>0.75</b>	<b>0.83</b>	<b>0.96</b>	<b>1.00</b>

Table 3. **Results of the motion-only action classifier (MOAC) on the CMU-Mocap dataset.** We compare the MOAC accuracies of our method to SOTA methods. We observe that the trend is similar to H36M, as we achieve higher accuracies than SOTA methods.

#### 4.5. Ablation Study on Keypose Retrieval Methods

We evaluate the effect of using keyposes obtained via different strategies: sampling, clustering and ours. The naive-sampling method evenly samples the motion at a rate of 15 frames, which is the average keypose duration from our method. The keyposes are then clustered without any keypose pruning. This method also doesn't require predicting durations, as the duration will always be 15. We also evaluate naive-sampling-pruned, where the keyposes are found through naive sampling, and then pruned. The clustering method performs clustering on *every* pose in the sequence, rather than only on the poses found via our optimization strategy. Afterwards, the keyposes are pruned in the same manner as in our method.

As can be seen in Table 4, our keypose method achieves the highest MOAC accuracies. The comparison with the naive-sampling method emphasizes the importance of having variable-duration keyposes, as opposed to evenly sampling the motion. The comparison with the clustering method emphasizes the importance of optimizing for the keyposes.

Further ablation studies on the employed the training strategies, the number of clusters and the error threshold chosen for the keypose algorithm are provided in the supplementary material.

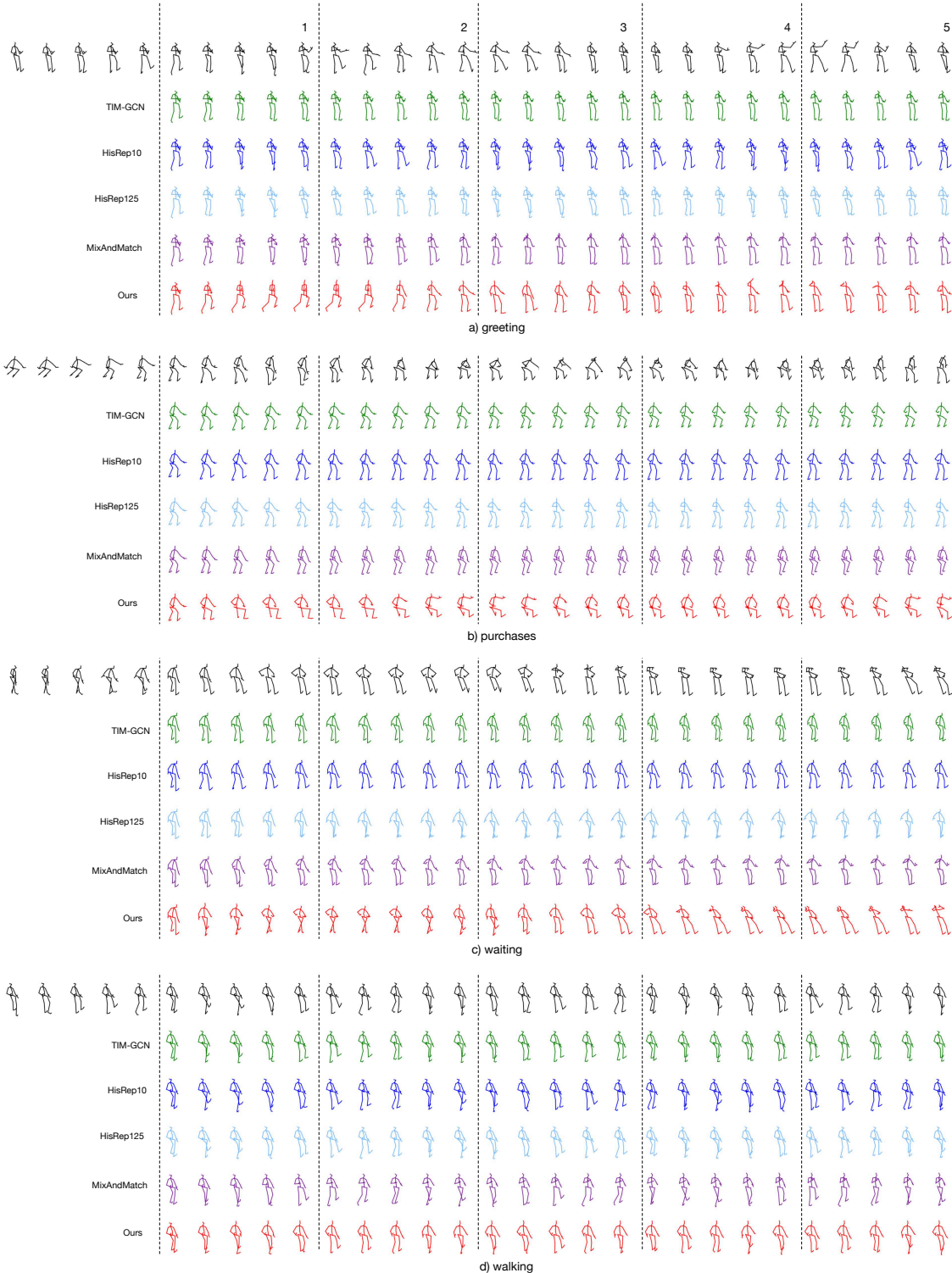


Figure 5. **Qualitative evaluation of our results** compared to SOTA ones, green: TIM-GCN, dark blue: HisRep10, light blue: HisRep125, violet: MixAndMatch, red: Ours. For the multiple prediction methods, ours and MixAndMatch, we display the prediction that has the lowest MPJPE error with respect to the ground truth. The top black row depicts the ground truth, and the first 5 poses are the conditioning ground truth. The numbers at the top indicate the future timestamp in seconds. We produce more dynamic poses for greeting, purchases and waiting, which are acyclic motions. For cyclic motions such as walking, the other methods are also able to produce dynamic poses.

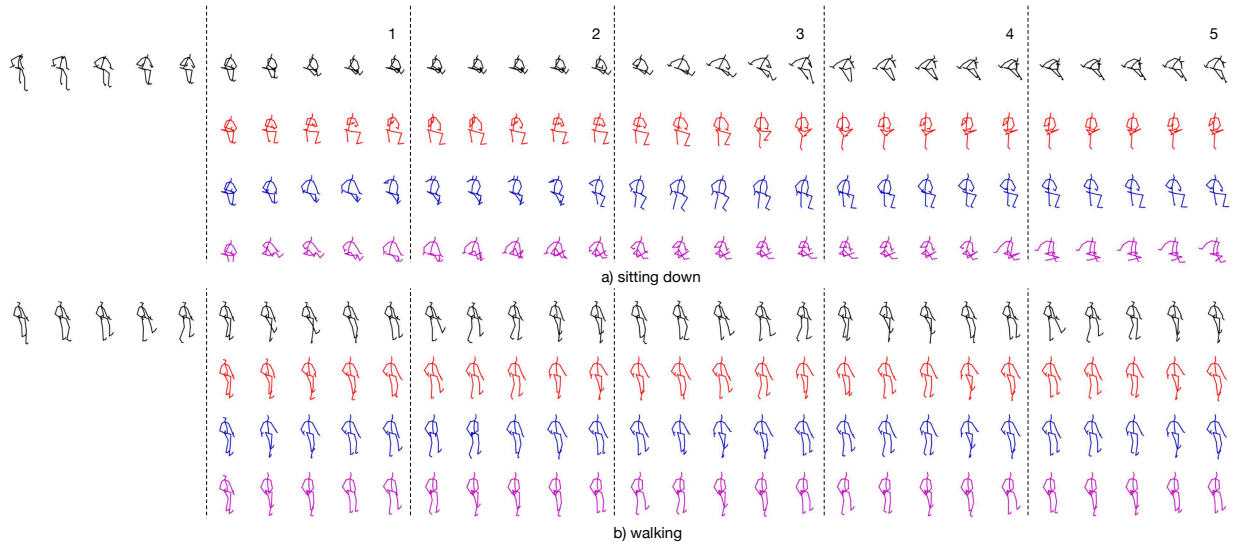


Figure 6. **Qualitative results of our multiple motion prediction** obtained by sampling the predicted label distribution. The numbers at the top indicate the future timestamp in seconds. The top row in black depicts the ground truth, and the remaining rows in color are our generated motions. The sampled motions are diverse, yet can all still be classified as “sitting down” and “walking”.

	top-1	top-2	top-3	top-5
Naive-sampling	0.28	0.38	0.51	0.67
Naive-sampling-pruned	0.30	0.42	0.52	0.63
Clustering	0.24	0.37	0.48	0.66
Ours	<b>0.33</b>	<b>0.45</b>	<b>0.55</b>	<b>0.70</b>

Table 4. **Analysis on the method of obtaining keyposes.** We compare the MOAC accuracies of different keypose methods: naive-sampling, naive-sampling-pruned, clustering and ours. The method we currently use achieves higher classification accuracies than the other two methods, indicating that the quality of the keyposes affects the performance.



Figure 7. **Examples of failure** to predict the correct keypose labels. The top example is from the category “posing”, however once our model detects the extended arms, it switches to the waving motion resembling the poses from the “greeting” category. The bottom example is from the category “sitting”. Though the motion of the legs are plausible, our prediction lifts a hand to its head, resembling a motion from the “phoning” category.

#### 4.6. Failure Modes

The main failure mode of our approach arises from incorrect cluster label prediction, as illustrated in Figure 7,

and from the fact that, while powerful, cluster centers cannot perfectly model all poses. To overcome this, we will study in future work the use of other clustering strategies such as the deep-learning based one of [30] that can be incorporated into our architecture for end-to-end training. We will also look into architectures better-tailored for processing long sequences, such as transformer networks [2].

## 5. Conclusion

To the best of our knowledge, our work constitutes the first attempt to predict diverse futures for long-term durations of 5 seconds. Our method is built on predicting pairs of keypose labels and durations. Using these, we reconstruct the motion via linear interpolation. To evaluate our results, we have introduced a new action classifier, MOAC, that specifically focuses on the transitions between poses, thus placing an emphasis on the correctness of *motion*, rather than that of *poses*. Our experiments have evidenced that our method yields more dynamic and realistic poses than the recent SOTA work, even when tailored to learn patterns for long term prediction. Furthermore, our approach lets us easily sample diverse future motions.

In future work, in addition to the improvement suggested in Section 4.6, we will look into deploying this technology into drones that attempt to follow people and to place themselves into the ideal position to capture their 3D pose [17]. This is an ideal application for this approach because it absolutely requires the ability to predict future poses far enough into the future for the drone to have the time to take advantage of the prediction.

## References

- [1] S. Aliakbarian, F. S. Saleh, M. Salzmman, L. Petersson, and S. Gould. A Stochastic Conditioning Scheme for Diverse Human Motion Prediction. In *Conference on Computer Vision and Pattern Recognition*, 2020. 2, 5, 6, 12
- [2] A. Vaswani, N. Shazeer, N. Parmar, J. Uszkoreit, L. Jones, A. N. Gomez, L. Kaiser, and I. Polosukhin. Attention is All You Need. In *Advances in Neural Information Processing Systems*, 2017. 8
- [3] E. Barsoum, J. Kender, and Z. Liu. HP-GAN: Probabilistic 3D Human Motion Prediction via GAN. In *Conference on Computer Vision and Pattern Recognition*, 2017. 2
- [4] S. Bengio, O. Vinyals, N. Jaitly, and N. Shazeer. Scheduled Sampling for Sequence Prediction with Recurrent Neural Networks. In *Advances in Neural Information Processing Systems*, 2015. 4, 11
- [5] J. Bütpege, M.J. Black, D. Kragic, and H. Kjellstrom. Deep Representation Learning for Human Motion Prediction and Classification. In *Conference on Computer Vision and Pattern Recognition*, 2017. 2
- [6] Judith Bütpege, Hedvig Kjellström, and Danica Kragic. Anticipating Many Futures: Online Human Motion Prediction and Generation for Human-Robot Interaction. In *International Conference on Robotics and Automation*, 2018. 1, 2
- [7] J. Bütpege, H. Kjellström, and D. Kragic. Predicting the What and How - A Probabilistic Semi-Supervised Approach to Multi-Task Human Activity Modeling. In *Conference on Computer Vision and Pattern Recognition*, pages 2923–2926, 2019. 2
- [8] CMU Graphics Lab Motion Capture Database, 2010. <http://mocap.cs.cmu.edu/>. 5
- [9] E. Corona, A. Pumarola, G. Alenyà, and F. Moreno-Noguer. *Context-aware Human Motion Prediction*. 2020. 2
- [10] J. Fan, X. Shen, and Y. Wu. Scribble Tracker: A Matting-Based Approach for Robust Tracking. *IEEE Transactions on Pattern Analysis and Machine Intelligence*, 34:1633–1644, 2012. 1
- [11] K. Fragkiadaki, S. Levine, P. Felsen, and J. Malik. Recurrent Network Models for Human Dynamics. In *International Conference on Computer Vision*, 2015. 2
- [12] P. Ghosh, J. Song, E. Aksan, and O. Hilliges. Learning Human Motion Models for Long-Term Predictions. In *3DV*, 2017. 1, 2, 5
- [13] L. Gui, K. Zhang, Y. Wang, X. Liang, J. M. F. Moura, and M. Veloso. Teaching robots to predict human motion. In *International Conference on Intelligent Robots and Systems*, 2018. 1
- [14] G. Habibi, N. Jaipuria, and J. P. How. Context-Aware Pedestrian Motion Prediction in Urban Intersections. In *arXiv Preprint*, 2018. 1
- [15] C. Ionescu, I. Papava, V. Olaru, and C. Sminchisescu. Human3.6M: Large Scale Datasets and Predictive Methods for 3D Human Sensing in Natural Environments. *IEEE Transactions on Pattern Analysis and Machine Intelligence*, 2014. 5
- [16] A. Jain, A.R. Zamir, and S. Savarese A. adn Saxena. Structural-Rnn: Deep Learning on Spatio-Temporal Graphs. In *Conference on Computer Vision and Pattern Recognition*, 2016. 2, 5
- [17] S. Kiciroglu, H. Rhodin, S. Sinha, M. Salzmman, and P. Fua. Activemocap: Optimized Viewpoint Selection for Active Human Motion Capture. In *Conference on Computer Vision and Pattern Recognition*, 2020. 1, 8
- [18] T. Lebailly, S. Kiciroglu, M. Salzmman, P. Fua, and W. Wang. Motion Prediction Using Temporal Inception Module. In *Asian Conference on Computer Vision*, 2020. 1, 2, 3, 5, 6, 12
- [19] M. Li, S. Chen, Y. Zhao, Y. Zhang, Y. Wang, and Q. Tian. Dynamic Multiscale Graph Neural Networks for 3D Skeleton Based Human Motion Prediction. In *Conference on Computer Vision and Pattern Recognition*, June 2020. 2, 5
- [20] Y. Li, L. Yuan, and N. Vasconcelos. Co-Occurrence Feature Learning from Skeleton Data for Action Recognition and Detection with Hierarchical Aggregation. In *International Joint Conference on Artificial Intelligence*, 2018. 5, 6, 13, 14
- [21] Wei Mao, Miaomiao Liu, and Mathieu Salzmman. History Repeats Itself: Human Motion Prediction via Motion Attention. In *European Conference on Computer Vision*, 2020. 1, 2, 3, 5, 6, 12
- [22] Mao, Wei and Liu, Miaomiao and Salzmman, Mathieu and Li, Hongdong. Learning Trajectory Dependencies for Human Motion Prediction. In *International Conference on Computer Vision*, 2019. 1, 2, 3, 5
- [23] J. Martinez, M.J. Black, and J. Romero. On Human Motion Prediction Using Recurrent Neural Networks. In *Conference on Computer Vision and Pattern Recognition*, 2017. 1, 2
- [24] J. Martinez, R. Hossain, J. Romero, and J.J. Little. A Simple Yet Effective Baseline for 3D Human Pose Estimation. In *International Conference on Computer Vision*, 2017. 5
- [25] R. Morais, V. Le, T. Tran, B. Saha, M. Mansour, and S. Venkatesh. Learning Regularity in Skeleton Trajectories for Anomaly Detection in Videos. In *Conference on Computer Vision and Pattern Recognition*, 2019. 1
- [26] D. Pavllo, D. Grangier, and M. Auli. Quaternet: A Quaternion-Based Recurrent Model for Human Motion. In *British Machine Vision Conference*, 2018. 3
- [27] Ian Simon and Sageev Oore. Performance rnn: Generating music with expressive timing and dynamics, 2017. 2
- [28] Bob Sturm, João Santos, Oded Ben-Tal, and Iryna Korshunova. Music transcription modelling and composition using deep learning. *Conference on Computer Simulation of Musical Creativity*, 04 2016. 2
- [29] S. Tang, M. Golparvar-Fard, M. Naphade, and M. Gopalakrishna. Video-based motion trajectory forecasting method for proactive construction safety monitoring systems. *Journal of Computing in Civil Engineering*, 34:04020041, 11 2020. 1
- [30] A. van den Oord, O. Vinyals, and K. Kavukcuoglu. Neural discrete representation learning. In *Advances in Neural Information Processing Systems*, volume 30, 2017. 8
- [31] B. Wang, E. Adeli, H.-K. Chiu, D.-A. Huang, and J. C. Niebles. Imitation Learning for Human Pose Prediction. In *International Conference on Computer Vision*, pages 7123–7132, 2019. 2

- [32] J. Zhang and C. Zong. Deep neural networks in machine translation: An overview. *IEEE Intelligent Systems*, 30(5), 2015. 2

# Long Term Motion Prediction Using Keypose - Supplementary Material

## 6. Supplementary Video

The supplementary video which can be accessed on <https://youtu.be/T1WjdF8ux6o> includes a short overview of our work. The motivation and methodology are briefly explained. We also compare videos of our qualitative results versus the results of the competing methods.

## 7. Ablation Studies

In our ablation studies, we report the MOAC accuracy results on the validation set as well as the test set. The validation accuracy reported is the sum of top-1, top-2, top-3 and top-5 OMAC accuracies on the validation set. For all cases, we chose our final model as the one obtaining the highest validation accuracy. Please note that the results presented here are not the average accuracies of multiple predicted motions. In order to evaluate quickly, we chose to predict a single future in a “greedy” manner: instead of sampling multiple futures from the predicted cluster probability distribution, we simply choose the one with the highest probability. We then report the average accuracies of these single predictions.

**Number of clusters** We report results of using different number of clusters in Table 5. Using too many or too few clusters leads to both lower validation and test accuracies. We also note that using more clusters leads to higher training time. We chose to use 1000 clusters in our final model.

**Keypose Error Threshold** The first step of the keypose extraction algorithm recursively selects keyposes from the sequence until the reconstruction error is below a threshold. In our experiments, we chose this number to be 500. We report results of using different error thresholds in extracting keyposes in Table 6. Using a threshold that is too low or high leads to lower validation accuracies. We also note that using a higher threshold leads to sparser keyposes, leading to a smaller training set. This allows for faster training, however the accuracy drops significantly when this threshold is set too high.

**Scheduled Sampling** For scheduled sampling, we use inverse sigmoid decay,

$$\epsilon_i = k / (k + \exp(i/k)) \quad (2)$$

as presented in [4] where  $k$  is the hyper-parameter of scheduled sampling and  $\epsilon_i$  is the probability that teacher forcing is performed in that iteration. Table 7 reports the results of using scheduled sampling for teacher forcing with varying  $k$ . We conclude that using scheduled sampling with  $k = 10$  gives the highest accuracies.

**Training Softmax Heat** During training, we tokenize our keyposes by passing the inverse distances of the keypose value to the cluster centers through a heated softmax function. In Table 8, we conduct an ablation study on the value of the heat. We observe that too much heat and too little heat both lead to low validation and test accuracies. In our experiments we set the softmax heat for training to 0.03.

**Sampling Softmax Heat** During inference, we predict multiple motions via sampling the predicted probability distribution passed through a heated softmax. The heat value of this softmax operation is studied in Table 9. We observe that using very little heat leads to higher accuracy and lower average MPJPE loss, due to the predictions becoming similar to the results of the greedy method. However, as the heat increases, the diversity of the multiple predicted motions also increases. This leads to a drop in accuracy, however the best MPJPE value also decreases. Therefore, in our evaluations we choose to set this value to 0.3, trading a bit of accuracy for more diverse predictions.

**Past Supervision** In Table 10, we analyze whether enforcing the loss on the outputs of the network as it processes the conditioning ground truth increases accuracy. We observe that this training strategy indeed increases both validation and test accuracies.

**Hidden Layer Size** Table 11 reports the results of using different hidden layer sizes. We choose 512 as it leads to higher accuracies.

**Noise** During training, we add noise to the inverse distances as a part of the keypose tokenization. In Table 12 we analyze the effects of this noise. We find that, indeed, adding a noise with standard deviation 0.1 is useful and increases accuracies.

	top-1	top-2	top-3	top-5	val-acc	training-time (hours)
100	0.24	0.37	0.47	0.66	2.45	1.36
250	0.28	0.41	0.51	0.68	2.48	1.54
500	0.30	0.42	0.52	<b>0.69</b>	2.58	1.78
1000 (Ours)	<b>0.34</b>	<b>0.45</b>	<b>0.55</b>	<b>0.69</b>	<b>2.61</b>	1.99
2000	0.32	0.43	0.52	<b>0.69</b>	2.52	2.23
3000	0.29	0.38	0.47	0.65	2.29	2.65

Table 5. **Ablation study on number of cluster centers** We observe that we have similar performance around using 1000 clusters, with 1000 giving the highest accuracy. As the number of clusters decreases, the training-time also decreases but the accuracy drops. This is caused by the final layer of the keypose network being a fully connected one, going from the hidden layer size (512) to the number of clusters. A decrease in the number of clusters therefore leads to a smaller network which is faster to train. An increased number of clusters also results in a drop of accuracy and also an increase in training-time.

	top-1	top-2	top-3	top-5	val-acc	training set size	training-time (hours)
300	0.29	0.38	0.49	0.66	2.48	12286	2.45
500 (Ours)	<b>0.34</b>	<b>0.45</b>	<b>0.55</b>	<b>0.69</b>	<b>2.61</b>	8760	1.99
750	0.32	0.41	0.51	0.66	2.50	5403	1.39
1000	0.32	0.42	0.50	0.64	2.28	3036	1.16

Table 6. **Ablation study on the error threshold for the keypose extraction algorithm.** We observe that we have similar performance around using 500 as the error threshold, with 500 giving the highest accuracy. As the error threshold decreases, the training-time increases because the size of the training set increases. As the error threshold increases, the training-time decreases as the set of keyposes becomes sparser. However the accuracy drops dramatically.

	top-1	top-2	top-3	top-5	val-acc
No-tf	0.30	0.43	0.53	0.67	2.49
Always-tf	0.31	0.42	0.53	<b>0.70</b>	2.49
$k = 10$ (Ours)	<b>0.34</b>	<b>0.45</b>	<b>0.55</b>	0.69	<b>2.61</b>
$k = 20$	0.33	0.43	0.54	0.69	2.54
$k = 60$	0.31	0.40	0.50	0.68	2.38
$k = 100$	0.32	0.40	0.49	0.66	2.38

Table 7. **Ablation study on the scheduled sampling** used for determining the probability of teacher forcing. We first evaluate the cases of not using scheduled sampling at all: either by not using teacher forcing at all during training (first row), or always using teacher forcing during training (second row). We then evaluate different cases of using scheduled sampling by varying the scheduled-sampling hyperparameter  $k$ . We observe that using scheduled sampling and setting the parameter  $k$  to 10 gives the best results in terms of validation and test accuracies in general.

	top-1	top-2	top-3	top-5	val-acc
heat = 0.01	0.28	0.41	0.49	0.69	2.44
heat = 0.02	0.30	0.42	0.50	<b>0.70</b>	2.51
heat = 0.03 (Ours)	<b>0.34</b>	<b>0.45</b>	<b>0.55</b>	0.69	<b>2.61</b>
heat = 0.04	0.33	0.43	0.52	0.68	2.58
heat = 0.07	0.29	0.40	0.50	0.68	2.57
heat = 0.1	0.30	0.41	0.52	0.68	2.54
heat = 1.0	0.24	0.35	0.45	0.63	1.94

Table 8. **Ablation study on the heat used during the heated softmax** operation of the label tokenization. We use the heat 0.03 during training as it gives the highest validation accuracy, which also corresponds to the highest test accuracies. We observe that when the heat is too small or too large, the validation accuracy drops significantly.

**Weights of loss functions** Table 13 reports the results of using different weights for the three loss functions we use. We find that setting these weights to  $w_{ce\text{-}soft} = w_{ce\text{-}hard} = 1.0$  and  $w_{duration} = 0.1$  leads to the highest accuracies.

## 8. Training-Time Analysis

We compare the training time of different methods in Table 14. We trained the methods of TIM-GCN [18] and HisRep [21] for 50 epochs and MixAndMatch [1] for 100k iterations, as recommended in their papers. We observe that

	test-acc	test MPJPE (ave)	test MPJPE (best)	val-acc	val MPJPE (ave)	val MPJPE(best)
heat = 0.05	<b>2.04</b>	237	218	<b>2.59</b>	<b>220</b>	206
heat = 0.1	<b>2.04</b>	<b>236</b>	210	2.58	221	204
heat = 0.3 (Ours)	2.03	<b>236</b>	199	2.55	223	187
heat = 0.5	1.99	<b>236</b>	<b>193</b>	2.51	223	<b>182</b>
heat = 1.0	1.63	<b>236</b>	196	2.02	227	<b>182</b>

Table 9. **Ablation study on the heat used during the softmax operation before sampling for multiple predictions.** We report the sum of top-1, top-2, top-3 and top-5 accuracies for both the validation and training set. We also report the average MPJPE and best MPJPE accuracies, as described in the main paper. We observe that as the heat decreases, the validation accuracy increases, and the average MPJPE loss decreases. However the minimum MPJPE loss also increases due to the sampled motions being less diverse and closer to the result of the greedy method. Therefore, we chose to use the heat 0.3 before sampling, as the validation accuracy was still quite high and the best validation MPJPE loss was low.

	top-1	top-2	top-3	top-5	val-acc
No-past-supervision	0.32	0.43	0.53	<b>0.69</b>	2.55
With-past-supervision (Ours)	<b>0.34</b>	<b>0.45</b>	<b>0.55</b>	<b>0.69</b>	<b>2.61</b>

Table 10. **Ablation study on supervising already seen keyposes.** We observe that supervising on the conditioning past also improves validation and test accuracies.

	top-1	top-2	top-3	top-5	val-acc
hidden size = 256	0.31	0.41	0.52	0.68	2.52
hidden size = 512 (Ours)	<b>0.34</b>	<b>0.45</b>	<b>0.55</b>	<b>0.69</b>	<b>2.61</b>
hidden size = 1024	0.32	0.42	0.51	0.66	2.59

Table 11. **Ablation study on the hidden layer size of the GRU cells.** We observe that using 512 as the hidden layer size leads to higher accuracies.

	top-1	top-2	top-3	top-5	val-acc
no-noise	0.28	0.38	0.47	0.60	2.31
noise = 0.05	0.31	0.42	0.52	0.67	2.51
noise = 0.1 (Ours)	<b>0.34</b>	<b>0.45</b>	<b>0.55</b>	<b>0.69</b>	<b>2.61</b>
noise = 0.5	0.19	0.32	0.41	0.58	2.48
noise = 1.0	0.14	0.23	0.34	0.53	1.48

Table 12. **Ablation study on the standard deviation of the Gaussian noise added to the inverse distances during keypose tokenization.** We observe that adding a noise of 0.1 increases accuracies, while using too much or too little noise leads to worse results.

	$w_{\text{duration}} = 0.1$					$w_{\text{duration}} = 1.0$				
	top-1	top-2	top-3	top-5	val-acc	top-1	top-2	top-3	top-5	val-acc
$w_{\text{ce-soft}} = 0, w_{\text{ce-hard}} = 1.0$	0.32	0.42	0.52	0.68	2.54	0.32	0.43	<b>0.55</b>	0.69	2.54
$w_{\text{ce-soft}} = 0.1, w_{\text{ce-hard}} = 1.0$	0.33	0.43	<b>0.55</b>	<b>0.71</b>	2.56	0.31	0.43	0.54	0.70	2.55
$w_{\text{ce-soft}} = w_{\text{ce-hard}} = 1.0$	<b>0.34</b>	<b>0.45</b>	<b>0.55</b>	0.69	<b>2.61</b>	0.32	0.43	0.54	0.70	2.57
$w_{\text{ce-soft}} = 1.0, w_{\text{ce-hard}} = 0.1$	0.32	0.41	0.52	0.67	2.56	0.33	0.44	<b>0.55</b>	0.70	2.55
$w_{\text{ce-soft}} = 1.0, w_{\text{ce-hard}} = 0$	0.32	0.42	0.53	0.68	2.54	0.31	0.43	0.54	0.70	2.55

Table 13. **Ablation study on the weights of different loss functions we use during training.** In the end, we chose the weight proportions of  $w_{\text{ce-soft}} = w_{\text{ce-hard}} = 1.0, w_{\text{duration}} = 0.1$  as this gave the highest validation accuracy.

our method is the fastest, with TIM-GCN also being relatively quick to train compared to the other methods.

## 9. Full Action Classifier

**Model** The full action classifier (FAC) is based fully on [20]. As opposed to the only-motion action classifier (OMAC), it also processed the poses in a separate stream. The two architectures are depicted in Figure 8.

**Results** We report the results of FAC on Human3.6M in Table 15. We note the high performance of the mean-pose predictor on this metric. This predictor produces a sequence consisting of a single pose, which is set to the mean pose of the action category. The mean poses of the action categories were found using the training set. Despite having no motion whatsoever, this predictor is able to outperform everyone, except for the oracle, which evaluates the ground truth future motion. We also point out that the static predictor,

	training-time (hours)
TIM-GCN	2.90
HisRep10	11.2
HisRep125	23.5
MixAndMatch	14.76
Ours	<b>1.99</b>

Table 14. **Training-time of different methods.** Our method is the fastest to train among state of the art motion prediction methods.

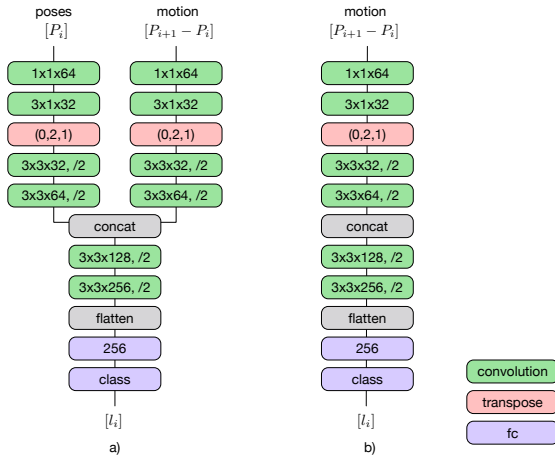


Figure 8. **Action classifier architectures** based on [20]. a) Full action classifier (FAC), which takes as input both the poses and the motion (difference between consecutive poses). b) Motion-only action classifier (MOAC), which takes only motion as input.

which predicts a sequence consisting only of the last-seen pose, also does relatively well on this metric. This predictor also produces no motion whatsoever.

While HisRep125 performs best out of the prediction methods, it had a much lower MOAC performance compared to our method. This indicates that the motions we predict are more realistic than the ones HisRep125 produces but that the FAC classifier can use a few well-predicted static poses to guess the motion nevertheless.

We also report the results of FAC on CMU Mocap Dataset in Table 16. The trend is similar to the results on Human3.6M, with the extremely high performance of the mean-pose predictor. This further leads us to conclude that this metric is able to distinguish sequences which have no motion at all, therefore not being a reliable metric for our purposes.

**Training Details** The action recognition models are trained to classify sequences of 125 frames (5 seconds). Both models are trained with Adam optimizer, using a learning rate of  $1e - 5$ , and weight decay of  $1e - 4$ . In order to make the model more robust to overfitting, we have added Gaussian noise during training to the input data. With independent probabilities of 0.5, a noise of 20 mm standard

	top-1	top-2	top-3	top-5
Oracle	0.59	0.78	0.86	0.94
Mean-Pose	0.53	0.67	0.73	0.80
Static	0.28	0.40	0.51	0.64
TIM-GCN	0.39	0.52	0.63	0.76
HisRep10	0.36	0.53	0.63	0.76
HisRep125	<b>0.42</b>	<b>0.56</b>	<b>0.67</b>	<b>0.80</b>
MixAndMatch (ave)	0.29	0.45	0.58	0.71
Ours (ave)	0.40	0.53	0.62	0.75

Table 15. **Results of the full action classifier (FAC) on the Human3.6M dataset.** We compare the classification accuracies of the motion predicted via our work compared to SOTA methods. The oracle evaluates ground truth future motions. Static evaluates a sequence consisting of only the last seen pose, i.e. not predicting any motion at all. Its relatively high performance despite being severely handicapped indicates that this is not a very reliable metric. Mean-pose evaluates a sequence consisting of a static pose set to the mean pose of the action category and is able to achieve results higher than everyone, emphasizing how little importance motion carries for this metric. HisRep125 achieves the best performance on FAC, whereas we achieve comparable results.

	top-1	top-2	top-3	top-5
Mean-Pose	1.0	1.0	1.0	1.0
Static	0.72	0.80	0.95	<b>1.0</b>
TIM-GCN	0.73	0.85	0.95	<b>1.0</b>
HisRep10	0.71	<b>0.90</b>	<b>0.98</b>	<b>1.0</b>
HisRep125	<b>0.74</b>	0.85	0.92	<b>1.0</b>
MixAndMatch (ave)	0.44	0.51	0.66	0.94
Ours (ave)	<b>0.74</b>	0.76	0.89	0.93

Table 16. **Results of the full action classifier (FAC) on the CMU Mocap Dataset.** The trend is similar to the results on Human3.6M. In this case, it is even more striking that the Mean-Pose predictor is able to get 100% accuracy on even top-1, with using just a single static pose. Static, which evaluates a sequence consisting of only the last seen pose also has a high performance rivalling the results of the learning-based prediction methods.

deviation is added to the motion and noise of 30 mm standard deviation is added to the poses. We have found that this procedure improves the validation accuracies. The trained models and the training code will also be released by us upon acceptance.

## 10. Cluster center visualization

We show a sample of 500 keypose cluster centers in Figure 9. It is necessary for them to be varied in order to be able to express the wide range of poses seen across different action categories. We find that the keypose cluster centers include poses from many categories, such as sitting, crouching, squatting, standing, walking, and making different arm gestures.

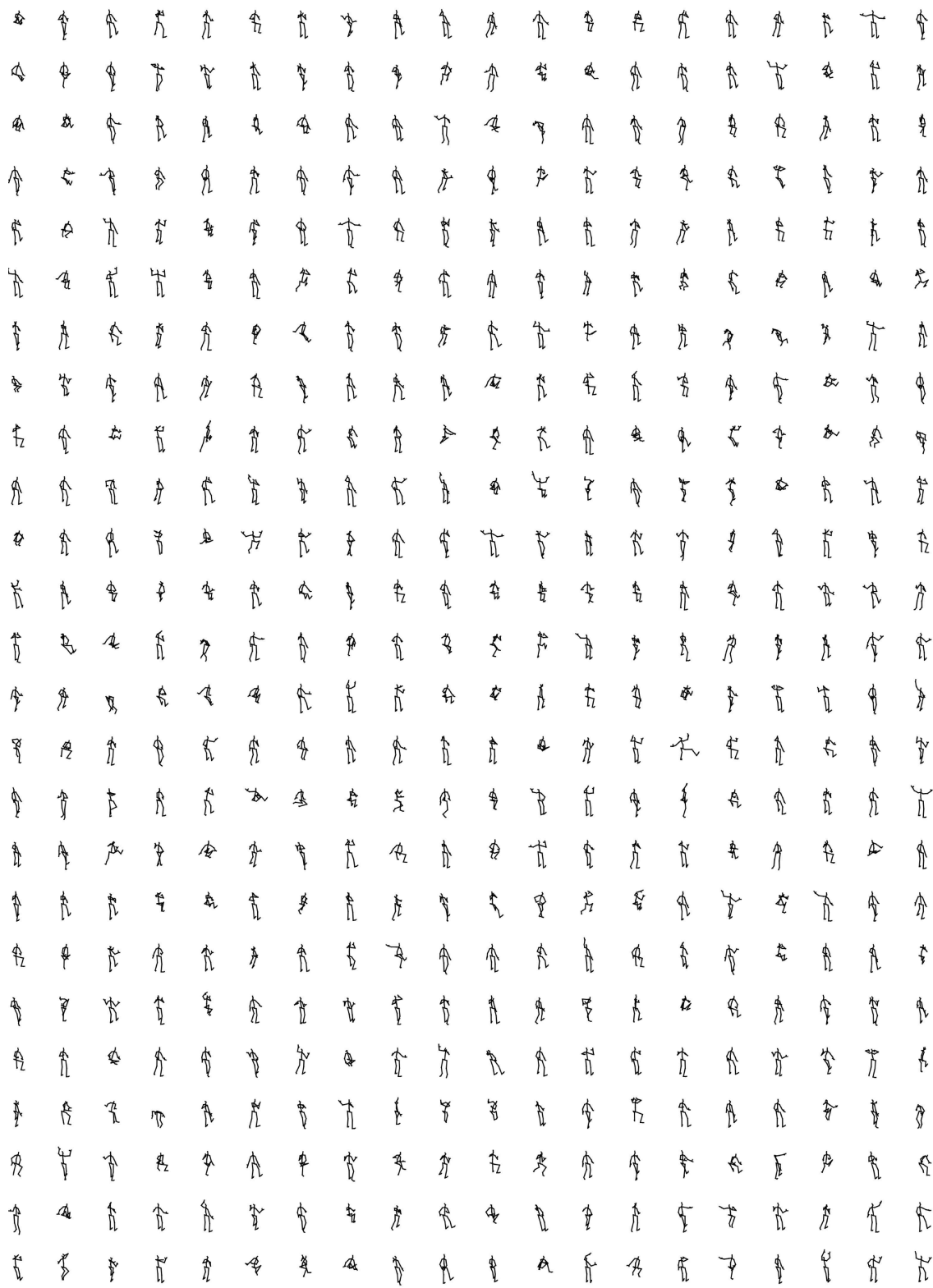


Figure 9. **Visualization of keypose cluster centers.** The sampled 500 keypose cluster centers here show that the cluster centers are quite varied and are able to represent the keyposes throughout the different categories of motions.

## 11. Additional Qualitative Results

Additional qualitative results on the Human3.6M dataset can be seen in Figures 10,11,12. The top row in black depicts the ground truth poses and the first five poses represent the last seen 1 second of the conditioning ground truth. We display the action categories which we were unable to show in our main paper due to lack of space. We again draw attention to the wide gestures our model is able to generate and the overall dynamism of the predicted motions as compared to the SOTA methods.

Qualitative results for the CMU-Mocap dataset can be seen in Figures 13,14. We see that we achieve more dynamic and realistic poses on this dataset as well.

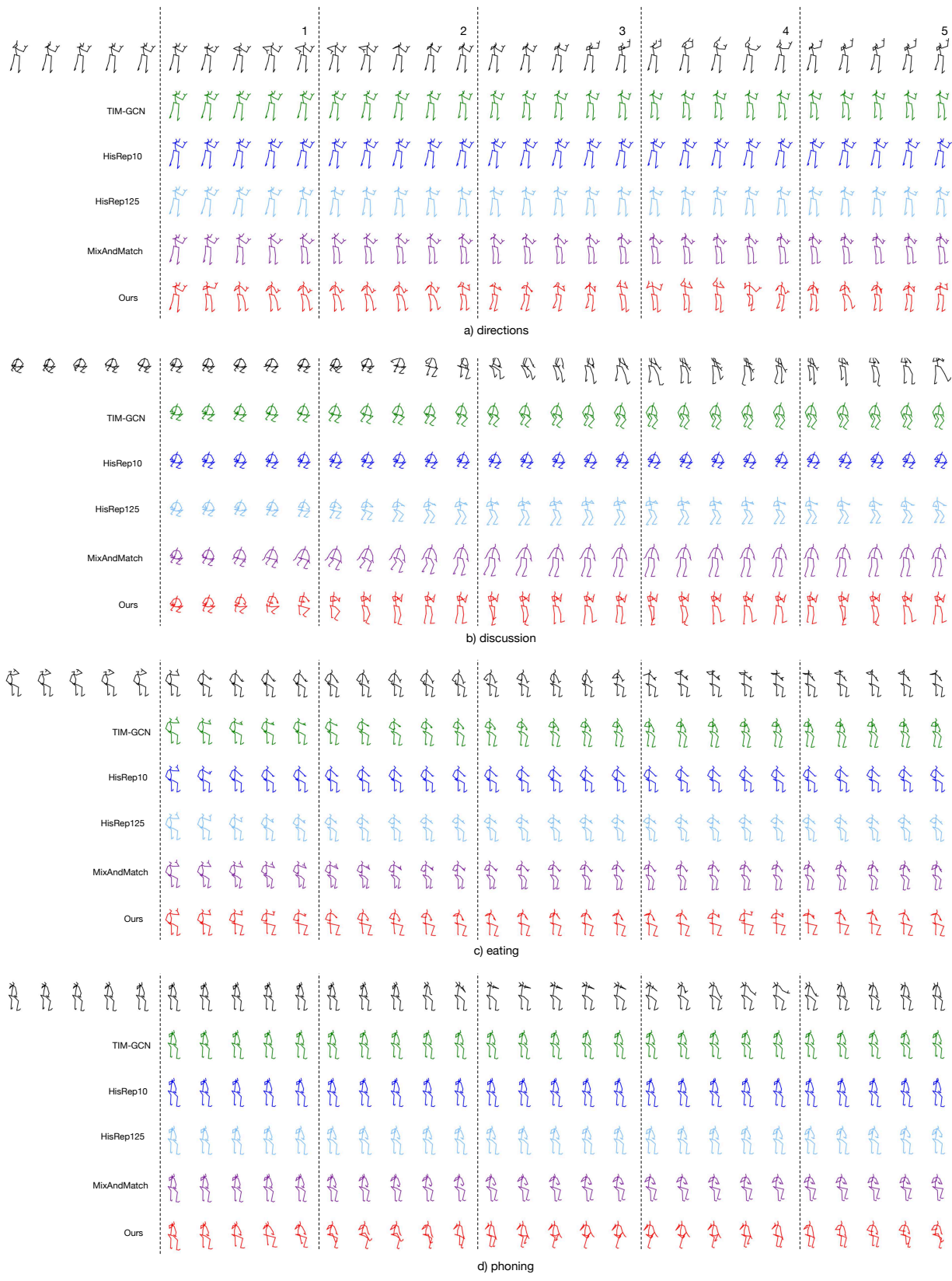


Figure 10. Qualitative results on Human3.6M of actions "directions", "discussion", "eating", "phoning".

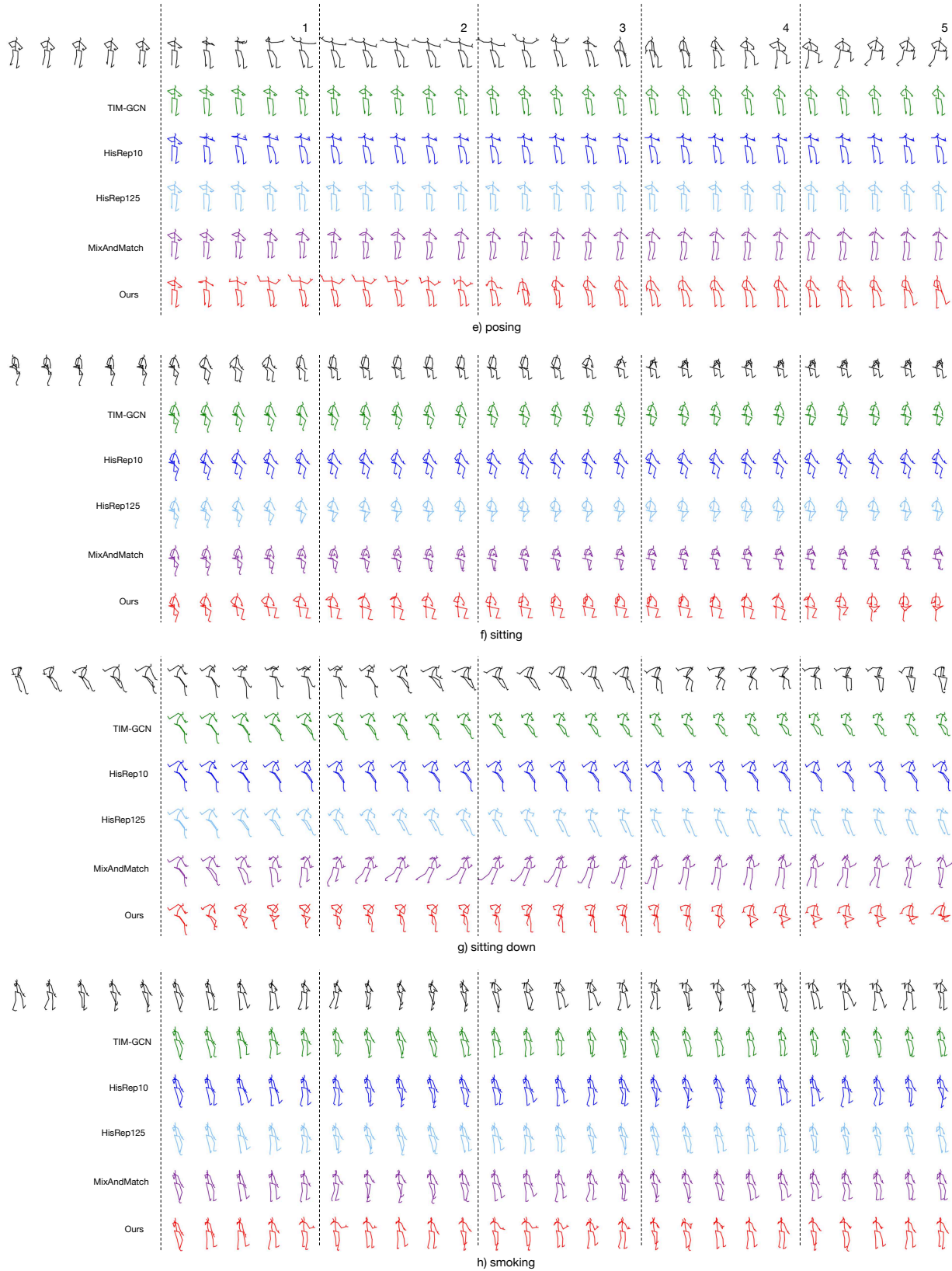


Figure 11. Qualitative results on Human3.6M of actions "posing", "sitting", "sitting down", "smoking".

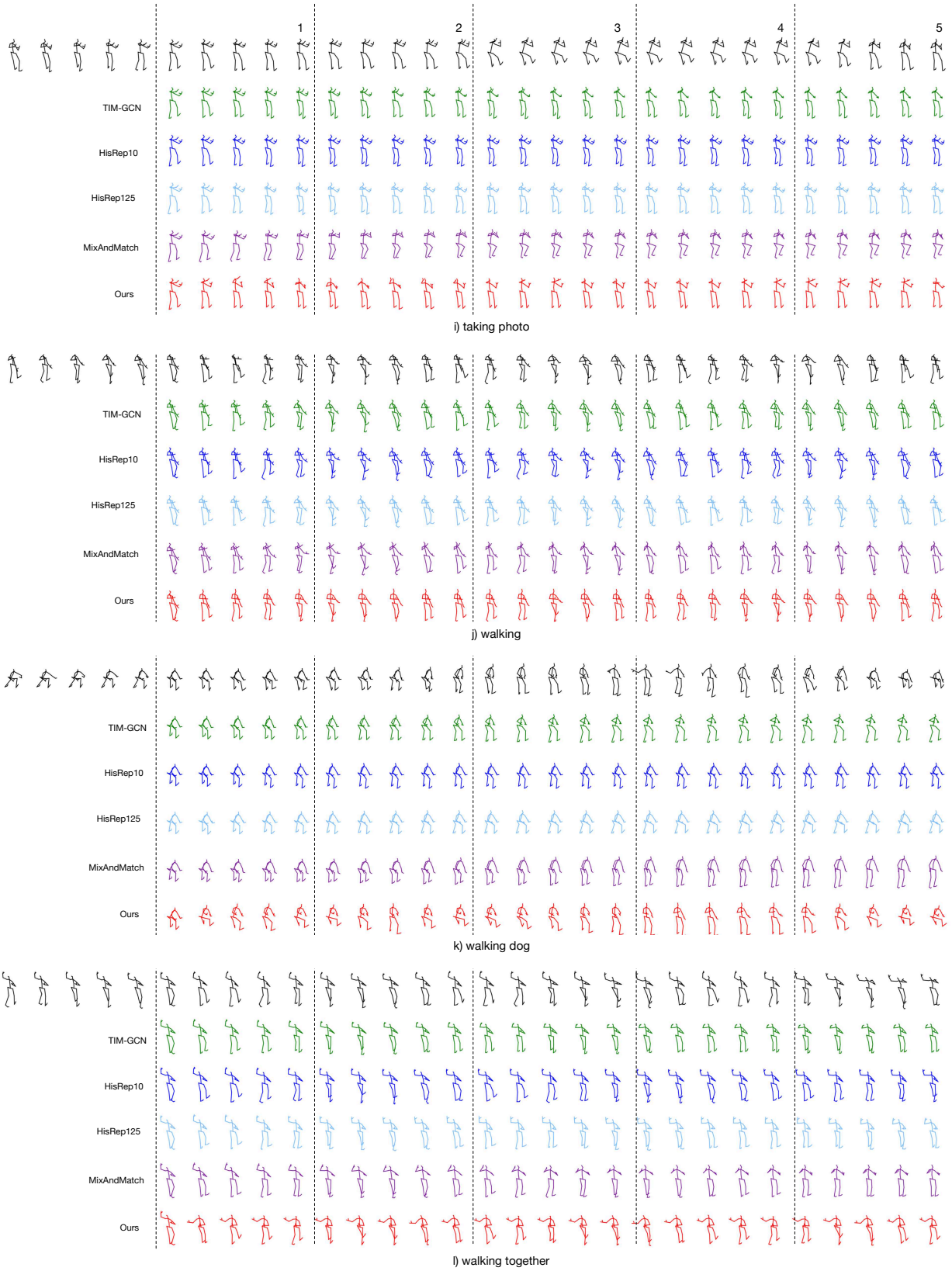


Figure 12. **Qualitative results on Human3.6M** of actions "taking photo", "walking", "walking dog", "walking together".

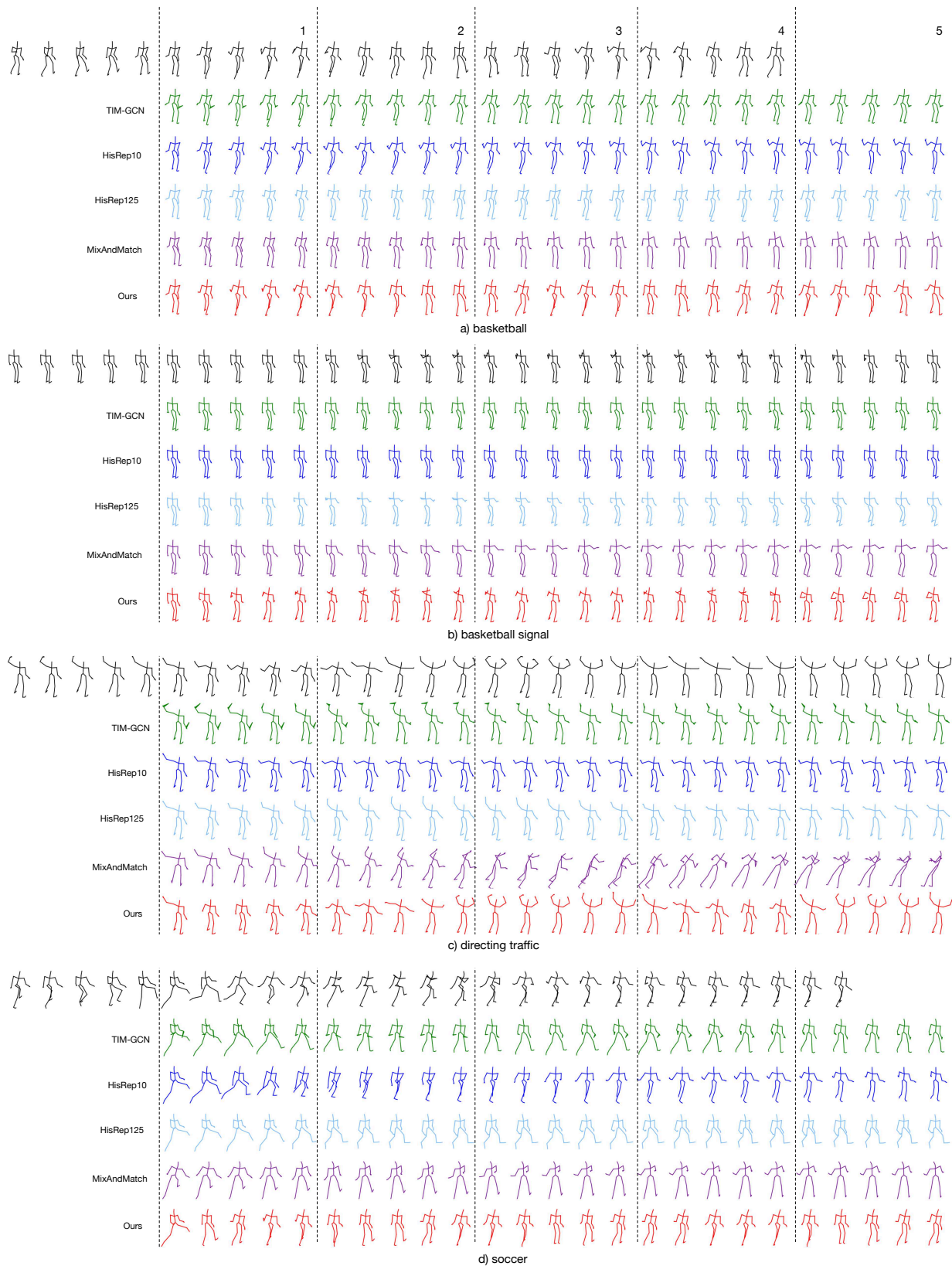


Figure 13. **Qualitative results on CMU Mocap** of actions "basketball", "basketball signal", "directing traffic", "soccer". We draw attention to the legs in basketball, the hands in basketball signal, the wide arm gestures in directing traffic and the legs in soccer.

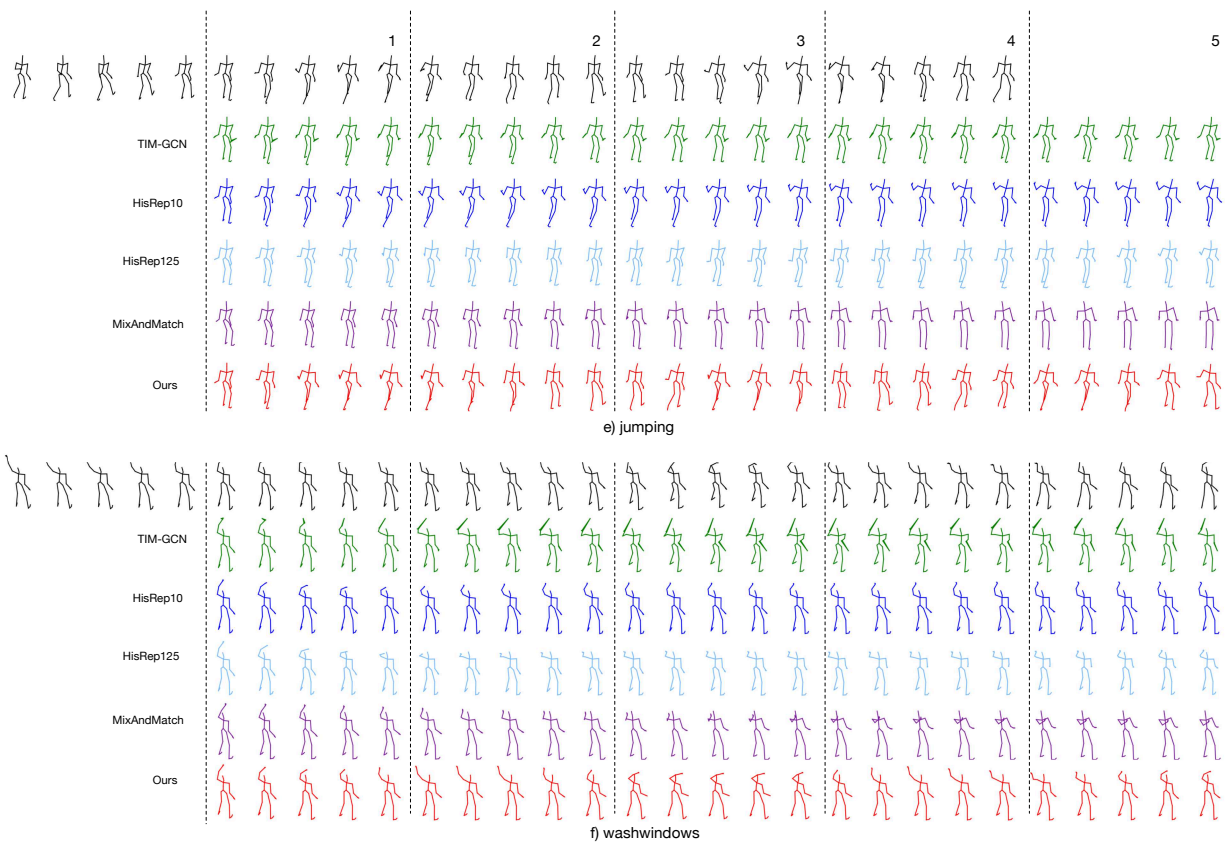


Figure 14. **Qualitative results on CMU Mocap** of actions "jumping","washwindows". We draw attention to the legs in jumping and the arms in washwindows.